HALO CLEANING AND COLLIMATOR OPTIMIZATION AT PERLE *

A. Cieplak[1†], A. Fomin[1], J. Michaud[1], A. Stocchi[1]
[1] Université Paris-Saclay, CNRS/IN2P3, IJCLab, Orsay, France
On behalf of the PERLE collaboration[‡]

Abstract

PERLE (Powerful Energy Recovery Linac for Experiments) is a multi-turn, high-current energy-recovery linac under development at IJCLab, designed to operate at 20 mA and 250 MeV. To limit beam-induced losses in downstream superconducting sections, halo particles must be intercepted at low energy. In this work, halo cleaning in the merger is studied using a 6D particle distribution obtained after the booster stage, at 7 MeV. The beam phase-space evolution is analyzed to identify optimal locations for one or two collimators. Particle tracking simulations performed with the Bmad code are used to validate the collimation strategy and quantify its efficiency. Despite the low dispersion in the merger, correlations between transverse and off-momentum halo enable partial removal of off-momentum particles. The sensitivity of the collimation efficiency to booster cavity misalignments is also investigated.

INTRODUCTION

High-current energy-recovery linacs such as PERLE [1], require careful control of beam losses to ensure reliable operation and to protect superconducting cryomodules [2]. Halo particles generated in the injector represent a primary source of potential losses and must be intercepted as early as possible, where the beam energy is still low.

The merger section is a natural location for such collimation. However, its optics is strongly constrained by the need to match Twiss parameters to the downstream lattice while controlling longitudinal properties such as R56 and dispersion [3, 4]. These constraints limit the flexibility to optimize collimation through conventional lattice tuning.

In this work, we adopt an alternative approach. Instead of adjusting the optics to predefined collimator locations, we analyze the evolution of a 6D halo distribution through the merger to identify the most effective positions for one or two collimators. A semi-analytical study is used to evaluate the collimation efficiency as a function of phase advance, providing insight into the optimal conditions for halo interception. This is complemented by particle tracking simulations using the Bmad code to identify optimal collimator positions and to quantify the achievable cleaning efficiency.

In addition, the sensitivity of the collimation performance to misalignments of the booster cavities is investigated.

* This work received government funding managed by the Agence Nationale de la Recheche (ANR) in the France 2030 framework - reference ANR-24-RRII-0001
Work supported by funding from European Union's program EU HORIZON-INFRA-2023-TECH-01-01 under GA n°101131435
† arnaud.cieplak@ijclab.in2p3.fr
‡ https://perle-web.ijclab.in2p3.fr/instituts/

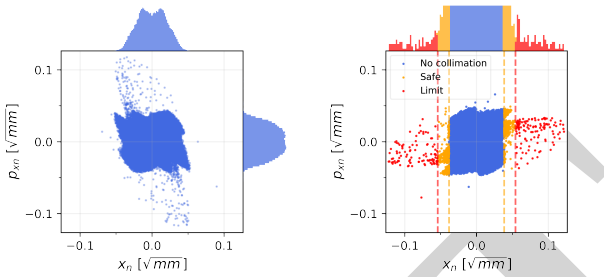

Figure 1: Beam profile in horizontal phase-space: at the beginning of Merger (left), at the optimal phase advance (right)

PHASE-ADVANCE ANALYSIS OF COLLIMATION EFFICIENCY

To study how the collimation efficiency depends on the phase advance, we use a 6D distribution at the booster exit, generated with OPAL (described in Ref. [5]). The distribution is transformed into normalized coordinates, as shown in Eq. (1), so that the analysis becomes independent of the local Twiss parameters.

$$x_n = \frac{x}{\sqrt{\beta_x}}, \quad p_{xn} = \sqrt{\beta_x}\, p_x + \frac{\alpha_x}{\sqrt{\beta_x}}\, x \tag{1}$$

In this representation, a rotation in the transverse phase space corresponds directly to a change in phase advance, allowing the collimation efficiency to be scanned as a function of phase advance only.

The initial distribution at the booster exit is shown in Fig. 1 (left), while Fig. 1 (right) shows the distribution at the phase advance that gives the best collimation performance. Particles are colored according to the applied collimation condition: blue for transmitted particles, orange for the ideal 2 kW cut, and red for the same cut with an additional safety retraction of 0.02 $mm^{1/2}$ in normalized coordinates.

The corresponding longitudinal phase-space projection shows that the transverse halo is correlated with the off-momentum tail, so a fraction of off-momentum particles is also intercepted (see Fig. 2).

Finally, the intercepted power is scanned as a function of phase advance for the considered collimator configuration (see Fig. 3). The baseline lattice is compared with the most pessimistic case among 1000 booster misalignment seeds. This scan identifies the phase advances that maximize halo interception and quantifies the sensitivity of the result to upstream cavity misalignments.

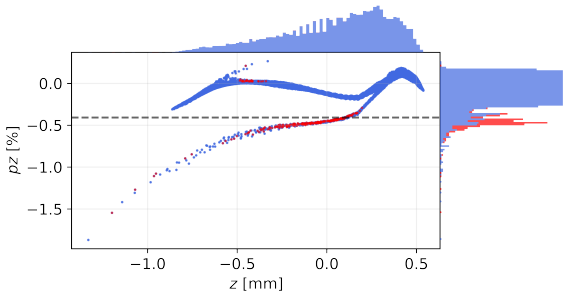

Figure 2: Longitudinal phase space. Transverse collimation

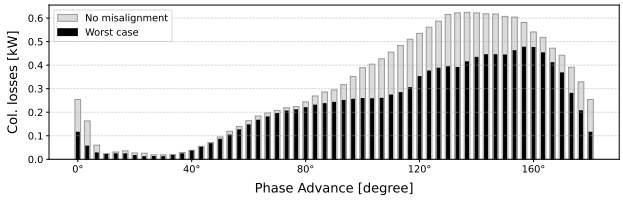

Figure 3: Power losses in collimator as a function of phase advance.

BMAD TRACKING STUDIES IN THE MERGER

To validate the phase-advance analysis of the previous section in the full merger lattice, particle-tracking simulations are performed with Bmad. The same set of 1000 six-dimensional distributions is used, each corresponding to a different booster-misalignment seed. For every seed, the merger optics is re-matched so that the beam can be transported from the booster and injected into the ERL loop while satisfying the main lattice constraints on dispersion, momentum compaction (R_{56}), Twiss matching at the downstream interface, and the beta-function limit at the cryomodule entrance.

The matched optics are shown in Fig. 4 for the ensemble of misalignment seeds. Each curve corresponds to one seed and illustrates the spread of the phase advance through the merger induced by booster misalignments. This spread quantifies the sensitivity of the collimation strategy to upstream errors.

Tracking is then carried out for each matched lattice. For each drift space between fixed lattice elements, the beam distribution is sampled at two reference positions: one located 5 cm after the beginning of the drift and one 5 cm before its end. These positions are treated as candidate collimator locations and are used to estimate the intercepted power for a given effective jaw opening. A 2 kW limit is applied to each collimator, together with a 0.5 mm safety margin to provide operational tolerance against potential beam excursions.

The resulting intercepted power is summarized in the corresponding scan. The solid curve represents the nominal lattice, while the shaded envelope covers the best and worst cases among the 1000 misalignment seeds. The tracking results are consistent with the phase-advance scan of Fig. 3: the intercepted power increases when the horizontal or vertical phase advance lies in the 120 –160 range, corresponding to the 2.73–3.28 m region. As expected, the beta function also

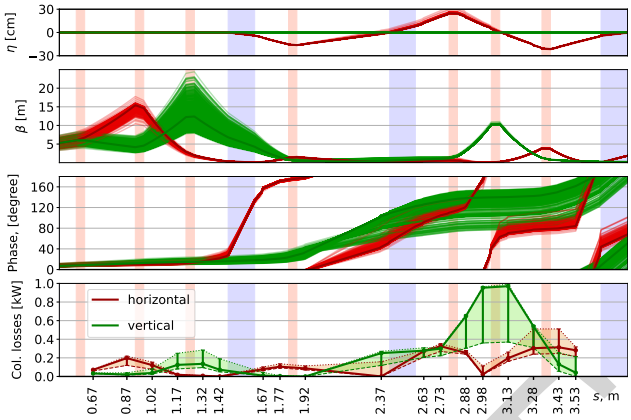

Figure 4: Optics and collimation performance along the merger. From top to bottom: dispersion, beta functions, phase advance (relative to the beginning of the merger), and intercepted power (including safety margin of 0.5 mm with respect to the 2 kW limit). Colors indicate horizontal (green) and vertical (red) planes. Orange and blue bands represent quadrupoles and dipoles, respectively.

plays an important role through its effect on beam size; at 2.98 m, the intercepted power in the horizontal plane drops because the beam is more strongly focused and the safety retraction moves the jaws outside the halo.

COLLIMATOR POSITION OPTIMIZATION AND PERFORMANCE MAPS

Horizontal and Vertical Halo Factor

In the previous section, the collimation efficiency was correlated with the power intercepted in the collimator. However, the power alone does not fully describe how effectively the halo is cleaned, since particles far from the core should be weighted more strongly than particles closer to the beam center. To capture this effect, we use the halo factor (see e.g. Ref. [6]) defined by Eq. 2.

$$H = \frac{\sqrt{3}}{2}\frac{\sqrt{I_4}}{I_2} - 2 \tag{2}$$

where H is the halo factor, I_2 and I_4, respectively the second and fourth momentum of the transverse distribution. This quantity provides a metric for the "cleanliness" of the remaining beam, since higher-order moments are more sensitive to particles at large amplitudes.

The two first maps in Fig. 5 show, for the horizontal and vertical planes, the worst halo factor obtained over the 1000 booster-misalignment seeds for each pair of collimator positions. The vertical and horizontal axes correspond to the positions of the first and second collimators, respectively, with the diagonal representing the case of a single collimator. The maps identify regions where the halo factor is minimized, i.e., where transverse cleaning is most effective. In the vertical plane, a single collimator located in the 2.63–3.28 m region is sufficient to achieve efficient halo

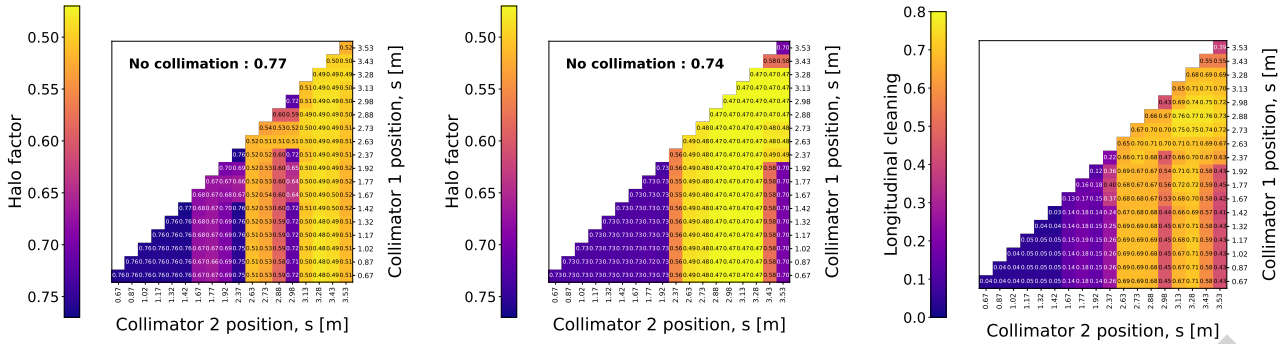

Figure 5: Two-dimensional maps of the halo factor for the horizontal plane (left), the vertical plane (center), and the longitudinal cleaning efficiency (right).

cleaning. Similarly, in the horizontal plane, a single collimator is also sufficient when placed in the 2.63–2.73 m or 3.13–3.53 m region. The halo factor is improved from initial values of 0.77 or 0.74 up to approximately 0.50, with slightly higher performance observed in the vertical plane.

Longitudinal Cleaning Efficiency

As shown in Fig. 2, transverse collimation also intercepts a fraction of the longitudinal halo because of the correlation between transverse amplitude and energy deviation. To quantify this effect, we define the longitudinal cleaning efficiency as

$$\eta_{\text{coll long}} \equiv \frac{N_{\text{coll}}(pz < pz_{\text{min}})}{N_{\text{tot}}(pz < pz_{\text{min}})} \tag{3}$$

where pz denotes the longitudinal momentum and pz_{min} defines the lower edge of the longitudinal halo considered in the analysis.

The third map in Fig. 5 shows the corresponding worst-case value of $\eta_{\text{coll long}}$ over the 1000 booster-misalignment seeds for each pair of collimator positions. The strongest longitudinal cleaning is obtained for a two-collimator configuration at (2.88 m, 3.28 m), where up to 77 % of the longitudinal halo is intercepted.

CONCLUSION

The study demonstrates that a collimation system in the PERLE merger effectively reduces the transverse halo and, through phase-space correlations, also mitigates the longitudinal halo.

The good agreement between the semi-analytical phase-advance analysis and Bmad tracking simulations provides a consistent basis for identifying optimal collimator locations.

For a single-collimator configuration, the optimal regions are 2.63–2.73 m and 3.13–3.28 m. To further improve longitudinal halo cleaning, two collimators can be combined, with the first placed in the 2.72–2.98 m region and the second in the 3.13–3.43 m region.

OUTLOOK

The physical implementation of the collimators requires robust cooling systems to handle the 2 kW heat load. Future simulations using Geant4 will determine the optimal collimator thickness and evaluate the shielding requirements associated with secondary radiation.

These results will support the mechanical integration of the collimation system within the accelerator lattice, taking into account both space constraints and radiation protection considerations.

REFERENCES

[1] D. Angal-Kalinin *et al.*, "Perle. powerful energy recovery linac for experiments. conceptual design report", *Journal of Physics G: Nuclear and Particle Physics*, vol. 45, no. 6, p. 065003, May 2018. doi:10.1088/1361-6471/aaa171

[2] O. A. Tanaka, T. Miyajima, N. Nakamura, T. Obina, M. Shimada, and Y. Tanimoto, "CollimatorÔÇÖs Impact Into the Transverse Emittance Growth at KEK Compact ERL", in *Proc. IPAC'19*, Melbourne, Australia, May 2019, pp. 174–177. doi:10.18429/JACoW-IPAC2019-MOPGW038

[3] S. A. Bogacz *et al.*, "PERLE - Lattice Design and Beam Dynamics Studies", in *Proc. IPAC'18*, Vancouver, Canada, Apr.-May 2018, pp. 4556–4559. doi:10.18429/JACoW-IPAC2018-THPMK105

[4] J. Michaud *et al.*, "Status of the beam dynamics studies for the PERLE Energy Recovery Linac", in *Proc. IPAC'25*, Taipei, Taiwan, Jun. 2025, pp. 702–705. doi:10.18429/JACoW-IPAC2025-MOPS041

[5] C. Monaghan and J. Michaud, "Characterisation of beam dynamics sensitivity to misalignments in the perle injector", in *Proc. IPAC'25*, Taipei, Taiwan, Jun. 2025, pp. 165–168. doi:10.18429/JACoW-IPAC2025-MOPB049

[6] C. K. Allen and T. P. Wangler, "Beam halo definitions based upon moments of the particle distribution", *Phys. Rev. Spec. Top. Accel. Beams*, vol. 5, no. 12, p. 124202, Dec. 2002. doi:10.1103/PhysRevSTAB.5.124202